Received: 4 October 2022 | Accepted: 2 November 2022

DOI: 10.1002/pamm.202200071

Factors influencing the dynamic stiffness in short-fiber reinforced polymers

Nicola Magino[1,*], **Jonathan Köbler**[1], **Heiko Andrä**[1], **Fabian Welschinger**[2], **Ralf Müller**[3], and **Matti Schneider**[4]

[1] Fraunhofer Institute for Industrial Mathematics ITWM, Kaiserslautern

[2] Robert Bosch GmbH, Renningen

[3] Technical University of Darmstadt

[4] Karlsruhe Institute of Technology (KIT)

In short-fiber reinforced polymers, fatigue damage is typically characterized by measuring the dynamic stiffness and its degradation under cyclic loading. Computational homogenization methods may be used to characterize the fatigue behavior of the composite via numerical predictions. Such an approach may reduce the *experimental* effort significantly. In the previous works, the authors proposed an elastic fatigue damage model for predicting the *relative* stiffness degradation of short-fiber reinforced materials. However, the absolute value of the dynamic stiffness within the first cycle showed deviations from the expected elastic material behavior. Thus, the effect of viscoelastic polymer behavior as well as different microstructure descriptors on the dynamic stiffness is studied in the work at hand.

1 Introduction

The stiffness properties of short-fiber reinforced polymers are influenced by a vast number of factors. Of primary importance is the underlying microstructure of the composite material. Commonly used statistical descriptors of the underlying microstructure of a short-fiber reinforced polymer (SFRP) are the fiber volume content, the fiber aspect ratio as well as the fiber orientation state, typically encoded by the second-order Advani-Tucker fiber orientation tensor [2].

Additionally, polymer and polymer-based materials are well-known to exhibit viscoelastic effects [10, 12]. The dynamic mechanical analysis (DMA) is a standard testing procedure to characterize the viscoelastic properties of the material and has been applied to both pure thermoplastics as well as reinforced thermoplastics to characterize the frequency dependent dynamic stiffness properties [14]. Under fatigue loading, the dynamic modulus serves as the quantity of interest when characterizing fatigue damage by experimental means. In a one-dimensional setting, it is defined as the secant between the extremal stress σ and strain ε in the direction of loading

$$E_{\mathtt{dyn}} = \frac{\sigma_{\mathtt{max}} - \sigma_{\mathtt{min}}}{\varepsilon_{\mathtt{max}} - \varepsilon_{\mathtt{min}}}. \tag{1}$$

We assume the matrix behavior under fatigue loading to be linear viscoelastic and aim to study the effect of different loading frequencies on the dynamic stiffness of the *reinforced* material behavior at high loading cycles. The fiber inclusions are considered to be linear elastic. We apply computational homogenization methods to predict the effective properties of a fiber structure. In a first step, we generate realizations of a layered fiber structure. Then, the material behavior of the constituents is prescribed. For viscoelastic materials, different approaches exist to derive the macroscale behavior [5, 9]. A convenient and computationally efficient method to predict the dynamic stiffness of a short-fiber reinforced structure is the approximate method introduced in Magino et al. [17]. It is based on assigning effective dynamic properties to the constituents of the material and deriving the *composite* behavior from elastic computations. We will refer to the approach as *single elastic computation* (SEC) approach in the remainder of this work.

2 Reference fiber structure and material

Experimental characterizations using μCT scans [11] of a commercially used polybutylene terephthalate (PBT) reinforced by short glass fibers and injected into a test plate with a depth of 2 mm are characterized by a layered fiber structure with fiber orientations as shown in Fig. 1. The fiber orientation is described by the components of the second order Advani-Tucker tensor A in its eigensystem. We use this layered structure as the reference for our sensitivity study. The fiber volume content in the specimen is known to be 17.8% on average. A constant fiber volume content over the depth of the specimen and a fixed aspect ratio of 29 is assumed for reference. The generated fiber structure is shown in Fig. 2.

* Corresponding author: e-mail nicola.magino@itwm.fraunhofer.de, phone +49 631 316004012

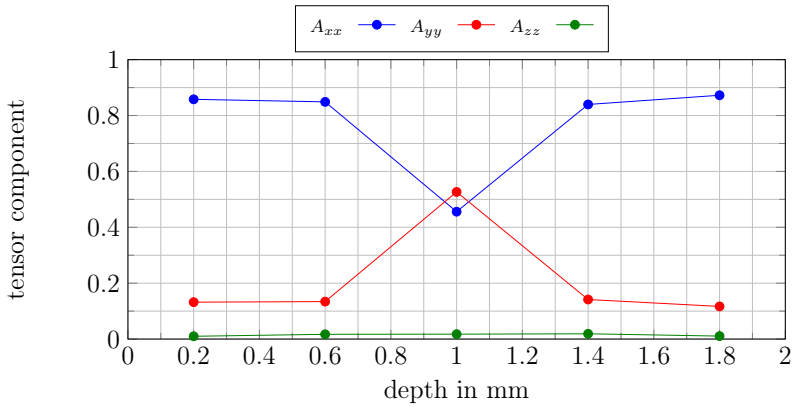

Fig. 1: Measured fiber orientation

Fig. 2: Realization of the layered fiber structure

3 Investigations on the influence of various factors on the dynamic stiffness

3.1 Influence of frequency

First, we shortly discuss the matrix and fiber material model in a three-dimensional setting, which is subsequently used to derive the long-term dynamic behavior of the composite is derived. Assuming the material behavior of the matrix to be linear viscoelastic, the stress-strain relation may be written in integral form as

$$\boldsymbol{\sigma}(x,t) = \int_0^t \mathbb{C}(x,t-u) : \frac{\partial \boldsymbol{\varepsilon}(x,u)}{\partial u} \mathrm{d}u, \tag{2}$$

where $\boldsymbol{\sigma}$ represents the stress tensor, $\boldsymbol{\varepsilon}$ denotes the strain tensor and $\mathbb{C}(x,t)$ refers to the material function of the material. The stress state at $\boldsymbol{\sigma}(x,0)$ is assumed to be zero and current stress state is obtained via integration over the time u up to the current time t. For the generalized Maxwell model [7], the latter assumes the form

$$\mathbb{C}(x,t) = \mathbb{C}_0(x) + \sum_{j=1}^{N} \mathbb{C}_j(x) \exp\left(-\beta_j t\right), \tag{3}$$

where $\mathbb{C}_i$ for $i \in \{0,\dots,N\}$ and β_j for $j \in \{1,\dots,N\}$ are quantities which depend on the underlying phase, i.e., they are different for fiber and matrix. For both fiber and matrix material, an universal Poisson's ratios ν independent of the index i is assumed, i.e., the tensors are given by

$$\mathbb{C}_i = E_i \left(\frac{\nu}{(1+\nu)(1-2\nu)} \mathbb{I} \otimes \mathbb{I} + \frac{\nu}{(1+\nu)} I^s \right), \tag{4}$$

where E_i denotes the Young's modulus of every tensor $\mathbb{C}_i$ and ν refers to the Poisson's ratio of the material. Here, $\mathbb{I}$ is the second-order identity tensor and I^s denotes the symmetric part of the fourth-order identity tensor. For the elastic fiber material, the Young's moduli with $i \geq 1$ are set to zero. Additionally, the relaxation times τ_i are defined as the inverse of β_i, i.e., $\tau_i = 1/\beta_i$.

For the long-term dynamic behavior of the composite material under periodic stress driven macroscopic loading,

$$\overline{\boldsymbol{\sigma}}(t) = \overline{\boldsymbol{\sigma}}_{\mathrm{a}} \cos(\omega t), \tag{5}$$

with the macroscopic stress amplitude $\overline{\boldsymbol{\sigma}}_{\mathrm{a}}$ and the angular frequency ω. Assuming small phase shifts of the matrix, the effective strain may be approximated in the form

$$\overline{\boldsymbol{\varepsilon}}(t) = \mathbb{S}^{\mathtt{eff}} : \overline{\boldsymbol{\sigma}}_{\mathrm{a}} \cos(\omega t - \delta) \tag{6}$$

with high accuracy as discussed in Magino et al. [17]. This formulation enables extending the one-dimensional definition for the dynamic stiffness (1) to a three-dimensional dynamic stiffness *tensor*. The approximation for the effective dynamic stiffness is based on the homogenization of an *elastic* material via the SEC approach. This enables us to efficiently estimate the frequency-dependent dynamic stiffness of the composite material at high cycles.

Element i	$E_i^{\mathtt{matr}}$ in GPa	$\tau_i^{\mathtt{matr}}$ in s	$\nu_i^{\mathtt{matr}}$	$E_i^{\mathtt{fiber}}$ in GPa	$\nu_i^{\mathtt{fiber}}$
0	2.475	-	0.4	72	0.22
1	0.582	2.4×10^{-3}	0.4		
2	0.430	2.4×10^{-2}	0.4		
3	0.316	2.2×10^{-1}	0.4		
4	0.233	1.9	0.4		

Table 1: Material parameters for Maxwell element number i of PBT matrix and glass fibers [17]

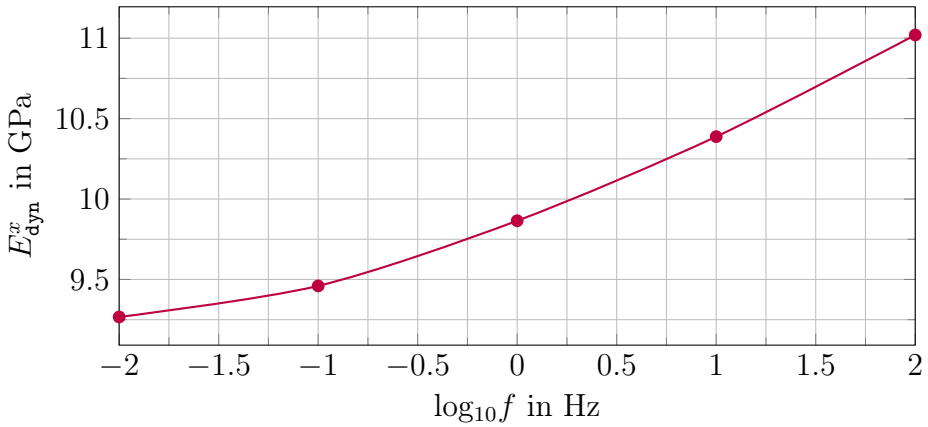

Fig. 3: Frequency dependence of the dynamic stiffness

The material parameters used are listed in Tab. 1 for matrix and fiber material.

In Fig. 3, the frequency dependence of the material is shown. The dynamic stiffness at high cycles depends significantly on the frequency. Indeed, it increases from 9.3 GPa at a frequency $f = 0.01$ Hz to 11.0 GPa at a frequency of $f = 100.0$ Hz, which is a relative increase of 18%. Thus, when modeling the dynamic stiffness of a short-fiber reinforced material, the frequency dependence is not to be neglected. Note that for further increasing frequencies the temperature increase in the test specimen becomes non-negligible. Hence, when investigating a broad range of frequencies, temperature effects should also be taken into account [1, 16].

3.2 Influence of fiber aspect ratio distribution

The dynamic stiffness dependent on the fiber aspect ratio distribution at a frequency of 1 Hz is evaluated. The average fiber aspect ratio $r_{\mathtt{a}}$ of the specimen is fixed to 29. However, due to manufacturing of components via an injection molding process, the aspect ratio may vary within the specimen. To study the effect of different fiber aspect ratios in every layer of an injection molded plate, we assume the aspect ratios to follow the distribution over the specimen thickness as shown in Fig. 4a. The fiber aspect ratio in every of the five layers of the structure is constant, but the aspect ratio between the different layers is different. The average aspect ratio throughout the whole specimen (averaged over the five layers) is kept at $r_{\mathtt{a}} = 29$. In two of the distributions, labeled as -4 and -2 in Fig. 4a, the aspect ratio in the center is below average by -4 and -2, respectively. In two other distributions, labeled as $+4$ and $+2$ in Fig. 4a, the aspect ratio in the center exceeds the average by $+4$ and $+2$, respectively. For each of the distributions, three fiber structures were realized and their dynamic modulus in x-direction is shown in Fig. 4b. Each computed dynamic stiffness is marked with a purple dot and the average over the three realizations for every aspect ratio is indicated by the black line.

The dependence of the dynamic modulus on the fiber aspect ratio is rather insignificant. Thus, this effect is assumed to be negligible.

3.3 Influence of fiber volume content distribution

The dynamic stiffness dependent on the fiber volume fraction distribution at a frequency of 1 Hz is evaluated. The average fiber volume fraction ϕ of the specimen is fixed to 17.8%. However, due to manufacturing of components via an injection molding process, the volume fraction may vary within the specimen. To study the effect of different fiber aspect ratios in every layer of an injection molded plate, we assume the fiber volume fraction to follow the distribution over the specimen thickness shown in Fig. 5a. The fiber volume fraction throughout the whole specimen (averaged over the five layers) is kept at $\phi = 17.8\%$. In two of the distributions, labeled as -4% and -2% in Fig. 5a, the volume fraction in the center is below average by -4% and -2%, respectively. In two other distributions, labeled as $+4\%$ and $+2\%$ in Fig. 5a, the volume fraction in the center exceeds the average by $+4\%$ and $+2\%$, respectively.

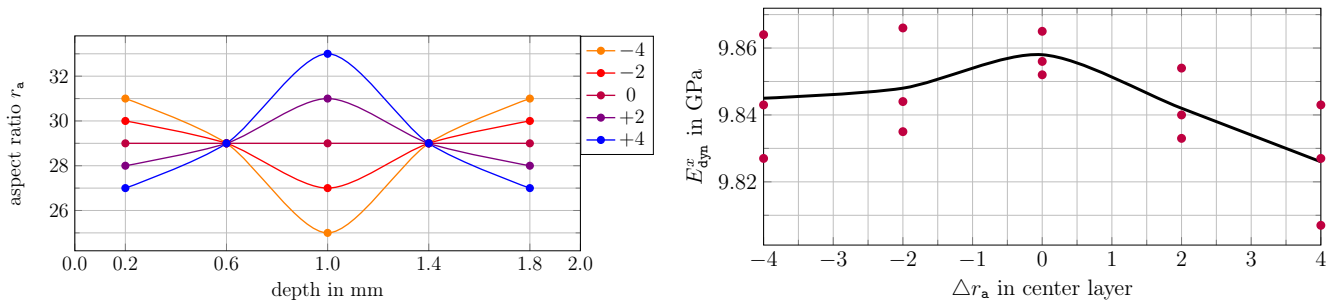

(a) Aspect ratio r_a over specimen thickness

(b) Dynamic stiffness

Fig. 4: Aspect ratio dependence of dynamic stiffness

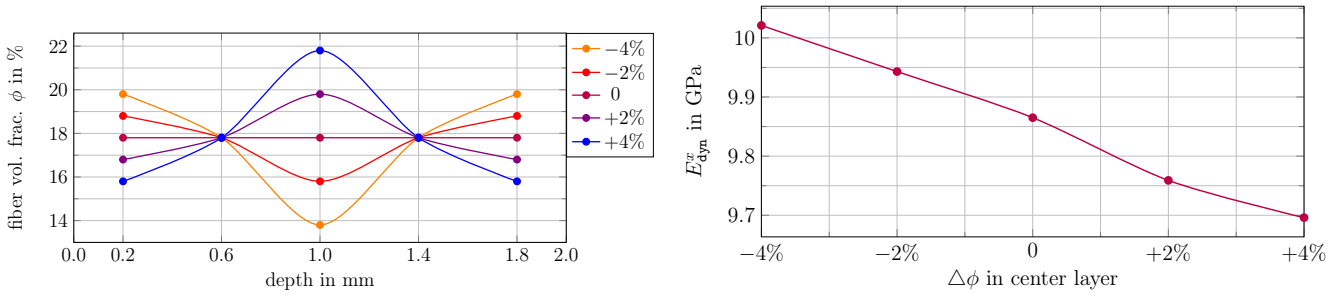

(a) Volume content ϕ over specimen thickness

(b) Dynamic stiffness

Fig. 5: Fiber volume content dependence of dynamic stiffness

For each of the discussed aspect ratio distributions, a realization is generated and its dynamic modulus in x-direction is evaluated and shown in Fig. 5b. One realization is assumed to be enough to show the trend of the fiber volume effect. The dependence of the evaluated dynamic stiffness on the fiber volume fraction distribution is significant. Compared to the structure with a 4% decreased fiber volume content in the center layer and a dynamic stiffness of 10.0 GPa, it decreases to 9.7 GPa for a by 4% increased fiber volume content in the center layer. Thus, within the examined range of volume fraction variations, we observe a relative deviation of 3%.

4 Implications for the upscaling technique

In recent years, FFT-based methods have been established as powerful tools for computational micromechanics. They make computational prediction of large fiber volume elements feasible [4,13]. However, when dealing with the prediction of a whole *component*, a direct coupling of micro- and macroscale still leads to excessively large computational costs. Thus, model order reduction methods may used to further decrease the computational effort in the online-phase.

The database method developed and applied to the prediction of the dynamic stiffness evolution in previous works [15, 18, 19] employs an NTFA approach and consists of the following steps:

1. discretization of the fiber orientation triangle into a finite set of orientations [9]
2. generation of a representative volume element (RVE) for the fatigue damage material law for each of the fiber orientations [8]
3. precomputation of several load cases on each of the RVEs [15, 18]
4. sampling of stress and damage solution fields for each of the structures
5. extraction of stress and damage modes via proper orthogonal decomposition for each of the structures
6. computation and storage of system matrices from the extracted modes.

Based on the precomputed and stored system matrices, an efficient and accurate online simulation of an engineering *component* based on an NTFA approach [3, 6] becomes feasible.

In the context of the viscoelastic fatigue damage model, the precomputed system matrices depend on the moduli and the Poisson's ratio as well as the loading frequency. In the case of matrix and fiber material sharing the same Poisson's ratio,

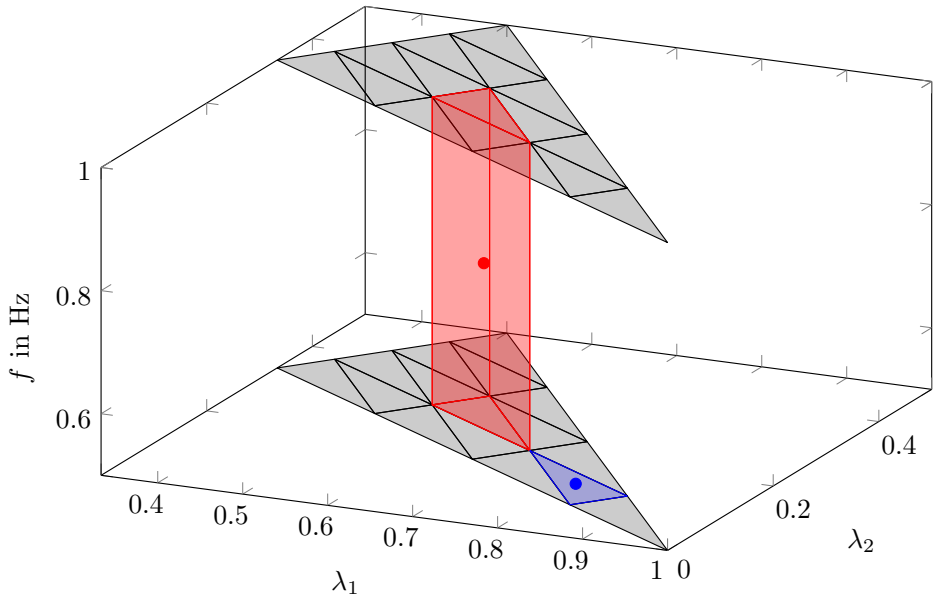

Fig. 6: Interpolation scheme

the effective moduli can be extracted from the material equations and a model order reduction based on a fiber interpolation scheme is possible. Otherwise the macroscopic potential depends on frequency dependent system matrices. Additionally, the system matrices strongly depend on the microstructure of the precomputed cells. Thus, incorporating a dependency of the fiber volume content increases the dimension of the space of considered microstructure characteristics. To be more specific, the number of parameters in the microstructure computations which *cannot* be explicitly extracted on the computation of the system matrices increases. For every of these parameters, a new dimension is added to the space of necessary precomputations.

The studies conducted in section 3 showed a non-negligible frequency and fiber volume content dependence of the composite material. Thus, the orginal two-dimensional interpolation concept based on the two largest eigenvalues of the fiber orientation needs to be extended to a multiple dimensional interpolation approach. This significantly increases the computational effort of the reduced order model as shown in Fig. 6. Here, the fiber orientation interpolation is shown for the elastic damage model discussed in previous works [18, 19] which was assume to solely depend on the fiber orientation in blue. The material response of any fiber orientation characterized by the eigenvalues λ_1 and λ_2 lying within the blue area can be predicted using an interpolation scheme built upon the three edges of the triangle. Thus, the prediction of the damage evolution at any fiber orientation requires the computation of *three* database points. In contrast, for increased dimensions of the parameter space, e.g., due to the choice of a viscoelastic material model, the effective model becomes dependent on an increasing number of precomputed structures. As shown in red in Fig. 6, to predict the material degradation at arbitrary frequencies (or any other additionally introduced parameter dimension), an interpolation between the *six* edges of the triangular prism needs to be applied, thus doubling the computational effort in the online computations. The computational effort increases prohibitively with the increase of parameter dependencies.

As a possible alternative, other interpolation schemes may be employed, e.g., using a tetrahedron. In that case the question on how to chose the four edges in the interpolation scheme arises. As a third option, a nearest neighbor approach may be employed. This approach is advantageous over the interpolation scheme in its computational effort in the online phase as the evaluation of only one fiber orientation is assumed to be sufficient for the prediction, in contrast to six orientations that need to computed in the interpolation approach. However, to meet a sufficient accuracy of the reduced order model, the number of fiber orientations necessary to precompute is expected to increase in comparison to the interpolation approach.

5 Conclusion

We studied the dependence of the dynamic stiffness of a short-fiber reinforced component on the frequency as well as the microstructural properties via computational means. We observed that the effective dynamic stiffness depends significantly on the frequency and the distribution of the fiber volume content, while the distribution of the aspect ratio has a less pronounced effect on the overall properties of the layered structure under investigation. This result gives guidance for further experimental and computational investigations on the dynamic stiffness of short-fiber reinforced polymers.

Acknowledgements Open access funding enabled and organized by Projekt DEAL.

References

[1] M. L. Williams, R. F. Landel, and J. D. Ferry, "The temperature dependence of relaxation mechanisms in amorphous polymers and other glass-forming liquids," *Journal of the American Chemical Society*, vol. **77**, pp. 3701-3707 (1955).

[2] S. G. Advani, and C. L. Tucker, "The Use of Tensors to Describe and Predict Fiber Orientation in Short Fiber Composites," *Journal of Rheology*, vol. **31** (8), pp. 751-784 (1987).

[3] J. C. Michel, and P. Suquet, "Nonuniform transformation field analysis," *International Journal of Solids and Structures*, vol. **40** (25), pp. 6937-6955 (2003).

[4] H. Moulinec, and P. Suquet, "A fast numerical method for computing the linear and nonlinear mechanical properties of composites," *CMAME*, vol. **157**, pp. 69-94 (1998).

[5] S. Staub, H. Andrä, M. Kabel, and T. Zangenmeister, "Multi-Scale Simulation of Viscoelastic Fiber-Reinforced Composite," *Technische Mechanik*, vol. **32** (1), pp. 70-83 (2011).

[6] F. Fritzen, and M. Leuschner, "Reduced basis hybrid computational homogenization based on a mixed incremental formulation," *CMAME*, vol. **260**, pp. 143-154 (2013).

[7] N. Rudolph, and T. A. Osswald, "Polymer Rheology - Fundamentals and Applications," *Hanser Publisher*, Munich, (2014).

[8] M. Schneider, "The Sequential Addition and Migration method to generate representative volume elements for the homogenization of short fiber reinforced plastics," *Computational Mechanics*, vol. **59**, pp. 247-263 (2017).

[9] J. Köbler, M. Schneider, F. Ospald, Heiko Andrä, and R. Müller, "Fiber orientation interpolation for the multiscale analysis of short fiber reinforced composite parts," *Computational Mechanics*, vol. **61**, pp. 729-750 (2018).

[10] K. Breuer, M. Schöneich, and M. Stommel, "Viscoelasticity of short fiber composites in the time domain: from three-phases micromechanics to finite element analyses," *Continuum Mechanics and Thermodynamics*, vol. **31**, pp. 363-372 (2019).

[11] P. A. Hessman, T. Riedel, F. Welschinger, K. Hornberger, and T. Böhlke, "Microstructural analysis of short glass fiber reinforced thermoplastics based on x-ray micro-computed tomography," *Composite Science and Technology*, vol. **183**, pp. 107752 (2019).

[12] D. Abdo, A. Gleadall, and V. V. Silberschmidt, "Damage and damping of short-glass-fibre-reinforced PBT composites under dynamic conditions: Effect of matrix behaviour," *Composite Structures*, vol. **226**, pp. 111286 (2019).

[13] M. Schneider, "A review of nonlinear FFT-based computational homogenization methods," *Acta Mechanica*, vol. **232**, pp. 2051-2100 (2021).

[14] C. Gómez, J. Mira, F. J. Carrión-Vilches, and F. Cavas, "Dynamic Moduli of Polybutylene Terephthalate Glass Fiber Reinforced in High-Temperature Environments," *Materials*, vol. **14**, pp. 483 (2021).

[15] J. Köbler, N. Magino, H. Andrä, F. Welschinger, R. Müller, and M. Schneider, "A computational multi-scale model for the stiffness degradation of short-fiber reinforced plastics subjected to fatigue loading," *CMAME*, vol. **373**, pp. 113522 (2021).

[16] V. Dorléans, R. Delille, D. Notta-Cuvier, F. Lauro, and E. Michau, "Time-temperature superposition in viscoelasticity and viscoplasticity for thermoplastics," *Polymer Testing*, vol. **101**, pp. 107287 (2021).

[17] N. Magino, J. Köbler, H. Andrä, F. Welschinger, R. Müller, and M. Schneider, "Accounting for viscoelastic effects in a multiscale fatigue model for the degradation of the dynamic stiffness of short-fiber reinforced thermoplastics" (submitted) (2022).

[18] N. Magino, J. Köbler, H. Andrä, F. Welschinger, R. Müller, and M. Schneider, "A multiscale high-cycle fatigue-damage model for the stiffness degradation of fiber-reinforced materials based on a mixed variational framework," *CMAME*, vol. **388**, pp. 1141981 (2022).

[19] N. Magino, J. Köbler, H. Andrä, F. Welschinger, R. Müller, and M. Schneider, "A space-time upscaling technique for modeling high-cycle fatigue-damage of short-fiber reinforced composites," *CSTE*, vol. **222**, pp. 109340 (2022).

